

PAPER

Half-mode substrate integrated plasmonic waveguide for filter and diplexer designs

To cite this article: Yue Cui *et al* 2022 *J. Phys. D: Appl. Phys.* **55** 125104

View the [article online](#) for updates and enhancements.

You may also like

- [Ultra-compact half-mode substrate integrated waveguide bandpass filters with IRCSRR metamaterial on reinforced hydrocarbon polymer ceramic composites](#)
Weilai Wang, Yong Mao Huang, Guoan Wang *et al.*
- [A hybrid substrate-integrated waveguide and spoof surface plasmon-polariton one-layer dual bandpass filter formed by resonant tunneling effect](#)
Zhang-Biao Yang, Dong-Fang Guan, Qingfeng Zhang *et al.*
- [Bandwidth enhancement of a half-mode substrate integrated waveguide filtering power divider using spoof surface plasmon polariton](#)
Ali-Reza Moznebi and Kambiz Afroz

ECS Toyota Young Investigator Fellowship



For young professionals and scholars pursuing research in batteries, fuel cells and hydrogen, and future sustainable technologies.

At least one \$50,000 fellowship is available annually.
More than \$1.4 million awarded since 2015!



Application deadline: January 31, 2023

Learn more. Apply today!

Half-mode substrate integrated plasmonic waveguide for filter and diplexer designs

Yue Cui¹, Kai-Da Xu^{2,*} , Ying-Jiang Guo³ and Qiang Chen¹

¹ Department of Communications Engineering, Tohoku University, Sendai, 980-8579, Japan

² School of Information and Communications Engineering, Xi'an Jiaotong University, Xi'an 710049, People's Republic of China

³ Microsystem and Terahertz Research Center, China Academy of Engineering Physics, Chengdu 610200, People's Republic of China

E-mail: kaidaxu@ieee.org

Received 3 October 2021, revised 29 November 2021

Accepted for publication 20 December 2021

Published 29 December 2021



Abstract

A half-mode substrate integrated waveguide (HMSIW) combined with spoof surface plasmon polariton (SSPP) structure is proposed to realize bandpass filter (BPF) characteristic and miniaturization, which is termed as the half-mode substrate integrated plasmonic waveguide (HMSIPW). Compared with the conventional HMSIW structure having identical cutoff frequency, this new design of HMSIPW not only supports SSPP modes, but also realizes a transversal size reduction of 19.4% and longitudinal reduction of more than 60%. Then, a diplexer based on two back-to-back placed HMSIPW BPFs is designed, and it has only one row of metallized via holes to further reduce the transversal size. The experimental prototypes of the filters and diplexer have been manufactured, and the measurement results agree well with simulation ones. Due to the size miniaturization and simple structure, the proposed designs will have many potentials in the integrated devices and circuits for wireless communication systems.

Keywords: bandpass filters, diplexers, dispersion curve, substrate integrated waveguide (SIW), miniaturization, spoof surface plasmon polariton (SSPP)

(Some figures may appear in colour only in the online journal)

1. Introduction

Substrate integrated waveguide (SIW) has the features of low fabrication cost, high power capability, low profile, strong anti-interference and high degree of integration, which is widely used in microwave and millimeter-wave circuits [1, 2]. At a certain dielectric thickness, the transversal dimension of the SIW determines its cutoff frequency, electromagnetic (EM) waves below this frequency cannot propagate through the SIW, which is similar to a high-pass filter (HPF). Due to the fixed transversal dimension of the SIW, it is difficult

to be used in the design of compact circuits with low operating frequencies. Moreover, since the propagation constant within the SIW is lower than the propagation constant of light in the same medium, the wavelength within the SIW becomes longer, which means that the SIW has a larger longitudinal dimension for a given electrical length. Therefore, it is necessary to investigate ways to reduce the dimensions of the SIW. In recent years, various new SIW structures have been presented in order to reduce the dimensions, such as ridge SIW [3], substrate integrated folded waveguide (SIFW) [4], half-mode SIW (HMSIW) [5] and ridged HMSIW (RHM-SIW) [6]. However, these works only reduce the transversal dimensions of the SIW, not the longitudinal dimensions.

* Author to whom any correspondence should be addressed.

In order to reduce both the transversal and longitudinal dimensions of the SIW simultaneously, slow-wave (SW) structure is introduced into the SIW [7, 8]. The cutoff frequency of the SIW is reduced due to the introduction of SW structure, which changes the effective permittivity and permeability of the overall structure. At the same time, since the phase velocity of the EM wave is slowed down by the SW structure, the longitudinal dimension of the SIW is reduced for a given electrical length. In [7], five rows of metallized via holes connecting only the bottom metallic layer are introduced as the SW structure between the two rows of metallized via holes of a conventional SIW. The cutoff frequency and phase velocity of EM wave are reduced due to the extra equivalent capacitance generated between the middle five rows of metallized via holes and the top metallic layer. In addition, the SW structure can also be achieved by modifying the metallic layer of the SIW, such as in [8], where the periodic poly-lines are etched in place of the top metallic layer of the SIW.

Surface plasmon polariton (SPP) is a special type of EM wave in the optical frequency band, which is confined to the interface between metal and dielectric, propagating in the direction parallel to the interface while decaying exponentially in the direction perpendicular to the interface [9]. To realize a SPP-like structure with high field-confinement capability in the microwave band, many periodic corrugated metallic structures have been proposed for the research on the spoof SPP (SSPP) [10–13]. Recently, SSPP has been increasingly used in microwave applications such as transmission lines [14–18], antennas [19–23] and filters [24–27]. Since the dispersion characteristics of SSPP can be adjusted by changing the geometric parameters, there are some structures that introduce SSPP as SW structures into SIWs to change the dispersions and cutoff frequencies of SIWs [28, 29]. In [28], a 2.5-D SSPP structure was introduced into the HMSIW, consisting of sub-wavelength slot lines etched into the HMSIW top metallic layer, a row of metallized via holes at the open side of the HMSIW, and metal patches on the bottom metallic layer of the HMSIW. The 2.5-D SSPP geometry parameters allow simultaneous adjustment of cutoff frequencies for waveguide mode and SSPP mode. However, the 2.5-D SSPP structure suffers from a complicated manufacturing. In [29], in order to reduce the size of the filter, a RHMSIW combined with SSPP structure is proposed. However, despite the reduction in longitudinal and transversal dimensions, the RHMSIW is thicker than HMSIW due to its structural feature.

In this article, a periodic E-shaped SSPP structure combined with an HMSIW is proposed to tailor the cutoff frequency and dispersion characteristics, which can be termed as the half-mode substrate integrated plasmonic waveguide (HMSIPW) and has been simply introduced in our previous work [30]. A high degree of freedom for adjusting the cutoff frequency and dispersion characteristics can be obtained. The proposed HMSIPW structure has the characteristics of a band-pass filter (BPF) since it combines the high-pass characteristic of HMSIW and the low-pass characteristic of SSPP. Simulation results show that the proposed HMSIPW structure

has a 19.4% reduction in the transversal dimension and over 60% reduction in the longitudinal dimension compared to the conventional HMSIW. Subsequently, a diplexer is designed based on the proposed HMSIPW BPF. The two HMSIPW BPFs are arranged back to back so that only one row of metallized via holes is required, further reducing the transversal dimension and manufacturing cost of the diplexer.

The remained parts of this article are organized as follows. In section 2, the design, analysis and discussion of the proposed HMSIPW BPF is presented. Then, a diplexer based on the two size-different HMSIPW BPFs is designed in section 3, along with its simulation and measurement. Finally, a brief conclusion is given in section 4.

2. HMSIPW filters

2.1. Configuration of the proposed HMSIPW BPF

Figure 1(a) shows the configuration of the proposed HMSIPW BPF, where the yellow regions denote the metallic area coating on the dielectric substrate and gray regions denote the metallized via holes. To clearly display the detailed configuration of the filter, the HMSIPW transmission part and the transition part from microstrip feeding to HMSIPW are shown in figures 1(b) and (c), respectively. In figure 1(b), the proposed HMSIPW structure consists of one dielectric substrate layer, two metallic layers and a row of metallized via holes. The dielectric substrate layer is sandwiched between the top and bottom metallic layers and the metallized via holes is inserted in the dielectric substrate layer to connect two metallic layers. An E-shaped slot array is etched on the top metallic layer as the SSPP structure. To clearly display the details of the HMSIPW structure, the schematic of one periodic element of the HMSIPW structure is also depicted in figure 1(b). The geometrical parameter h is the thickness of the dielectric substrate. The parameter w is the width of the proposed HMSIPW structure, and p is the length of the periodic element. The parameters a and b are the depths of the E-shaped transversal center slot and side slot, respectively, while c and w_s are the longitudinal length and width of the E-shaped slot, respectively. The parameter d is the diameter of the metallized via hole and parameter g is the distance between two adjacent via holes.

To achieve good impedance matching between 50 Ohm microstrip line (MSL) and HMSIPW, a transition structure is designed, as illustrated in figure 1(c). The transition structure includes two parts: Part I is the transition between MSL and HMSIW, and Part II is the transition between HMSIW and HMSIPW. In Part I, a tapering MSL on the top metallic layer is used for the impedance transition to the HMSIW. In Part II, impedance matching between the HMSIW and the HMSIPW is achieved by introducing three gradient E-shaped slots.

2.2. Dispersion analysis of the HMSIPW

The proposed HMSIPW BPF is designed on the FSD220G substrate ($\epsilon_r = 2.2$, $\tan\delta = 0.0009$) with a thickness of $h = 0.127$ mm, and the geometrical parameters of the proposed

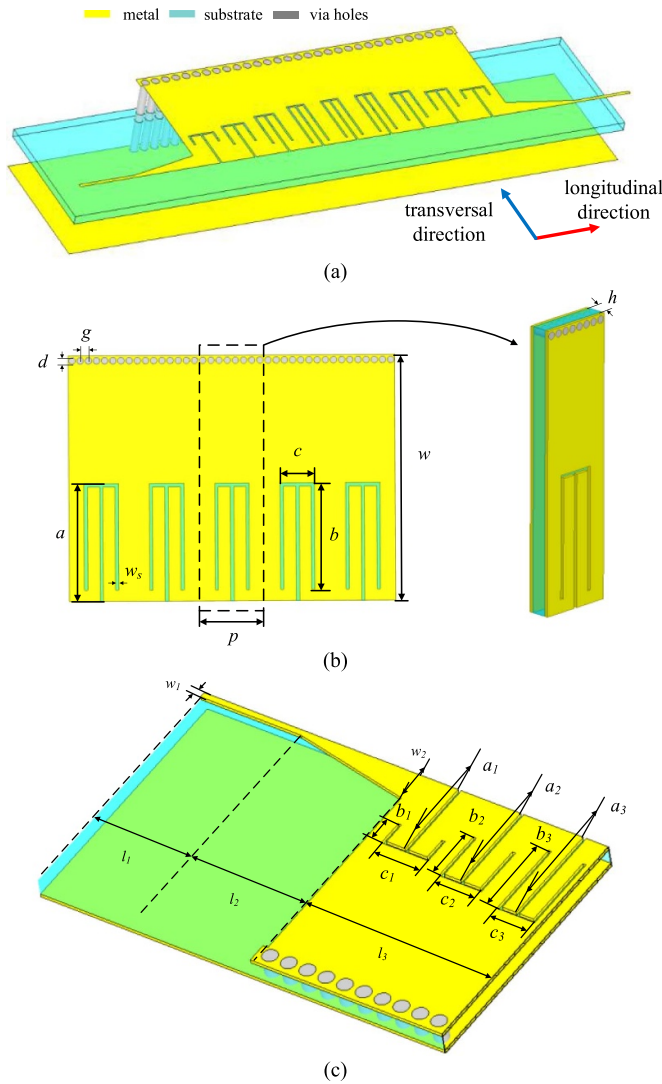


Figure 1. (a) Configuration, (b) transmission part and (c) transition part of the proposed HMSIPW BPF.

filter are shown in table 1. With the help of the eigenmode solver in CST Microwave Studio which is based on adaptive mesh refinement, we investigate the dispersion characteristics of the proposed HMSIPW structure (i.e. periodic array of the proposed HMSIPW element) with different geometrical parameters, as shown in figure 2, where k is the propagation constant in the direction of propagation. In figure 2(a), as w increases, the lower cutoff frequency gradually decreases, and the upper cutoff frequency is almost unchanged, which means the width of the HMSIW only affects the waveguide mode, without influence of the SSPP mode. Figure 2(b) presents the dispersion curves for different values of parameter a . It can be seen that as a increases, the upper cutoff frequency decreases, while the lower cutoff frequency remains essentially unchanged, indicating that the depth of the E-shaped middle transversal slot mainly affects the SSPP mode and has little effect on the waveguide mode. Figures 2(c) and (d) give the dispersion curves for different depths of the E-shaped

Table 1. Dimensions of the proposed HMSIPW BPF.

Para.	Dim. (mm)	Para.	Dim. (mm)	Para.	Dim. (mm)
w	14.5	w_1	0.37	l_1	6.5
p	4	w_2	1.9	l_2	7.5
w_s	0.2	a_1	5	l_3	13
d	0.9	a_2	5.67	c_1	2.6
g	0.3	a_3	6.33	c_2	2.3
a	7	b_1	1.6	c_3	2
b	6.5	b_2	3.23		
c	1.7	b_3	4.87		

The Para. in the table means the parameter and the Dim. is the dimension.

slot (i.e. b and c), which can be observed that the larger the parameters b and c , the lower the cutoff frequencies of waveguide mode and SSPP mode. This phenomenon is due to the larger equivalent capacitance and inductance introduced by increasing dimensions of the SSPP, which will be discussed in details in section 2.4. As the lower cutoff frequency is decreased but the width of HMSIW remains unchanged, the transversal size reduction of the HMSIPW structure can be obtained by changing the depths of the E-shaped two-sides transversal slots and longitudinal slot.

The dispersion comparisons among the proposed HMSIPW, a conventional HMSIW with identical lower cutoff frequency, and a E-shaped SSPP with identical dimensions are illustrated in figure 3. The dispersion curve of HMSIW indicates a high-pass feature, while that of E-shaped SSPP indicates a low-pass feature. Obviously, the proposed HMSIPW has the dispersion features of both HMSIW and E-shaped SSPP, which means it has a bandpass filtering feature. In addition, it can be seen from the figure 3 that the transversal length of the HMSIW is 18 mm, while the transversal length of the HMSIPW is 14.5 mm, which shows that the HMSIPW proposed in this section has a transversal reduction of 19.4% compared to the conventional HMSIW.

To further investigate the dispersion characteristics of the proposed HMSIPW, the comparisons of the dispersion curves of the proposed HMSIPW and the conventional HMSIPW with different depths of the SSPP slot are given in figure 4, where the two HMSIPW structures are set with the same width (w). It can be seen that the proposed HMSIPW has smaller lower and upper cutoff frequencies (i.e. better transversal reduction) than the conventional HMSIPW, even under the condition of the SSPP slot with the deepest depth ($a = 13$ mm), which proves that the proposed HMSIPW has a stronger field confinement compared with the conventional HMSIPW.

The desired BPF based on the proposed HMSIPW can be designed through the following three steps: Firstly, change the dimensions of the E-shaped two-sides transversal slots and one longitudinal slot (i.e. parameters b and c) to get the specific lower cutoff frequency. Then, adjust the depth of the E-shaped middle transversal slot (i.e. parameter a) to get the desired upper cutoff frequency. Lastly, according to the parameters of the HMSIPW structure obtained from the above two steps, we can add the transition structure to construct the BPF with

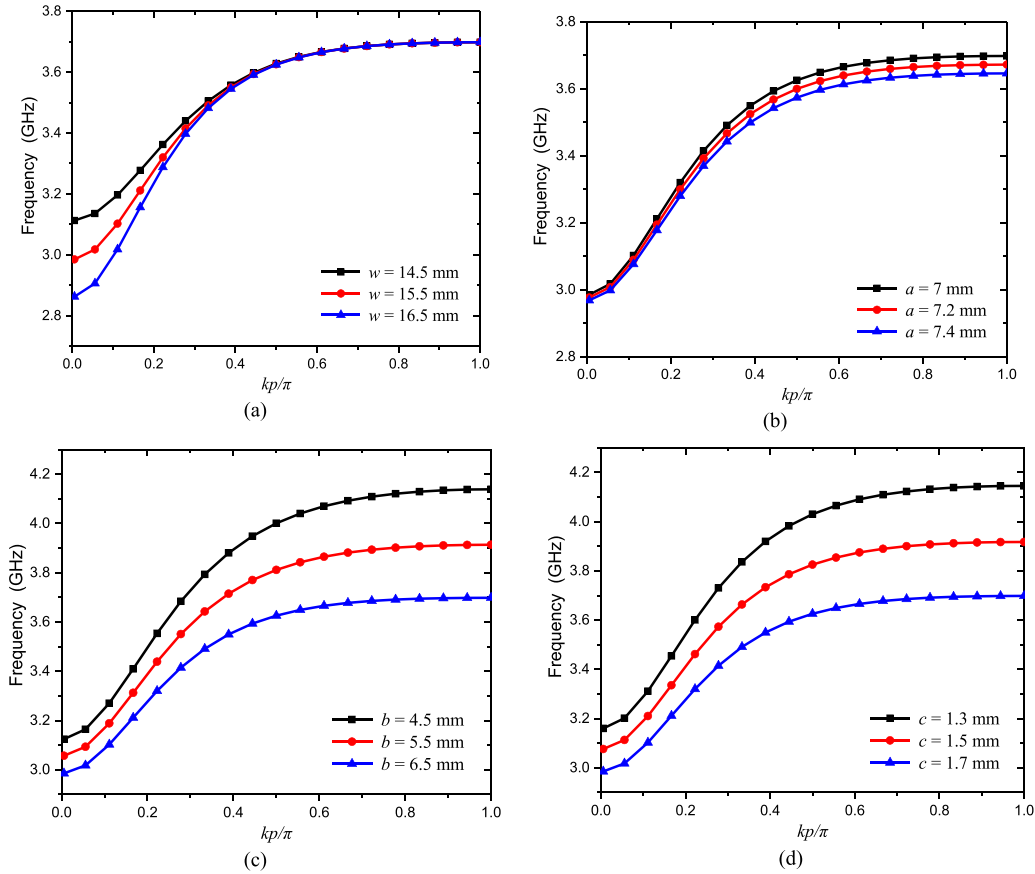


Figure 2. Dispersion curves of the proposed HMSIPW with different (a) widths of the HMSIW w , (b) depths of the E-shaped middle transversal slot a , (c) depths of the E-shaped two-sides transversal slots b and (d) depths of the E-shaped longitudinal slot c .

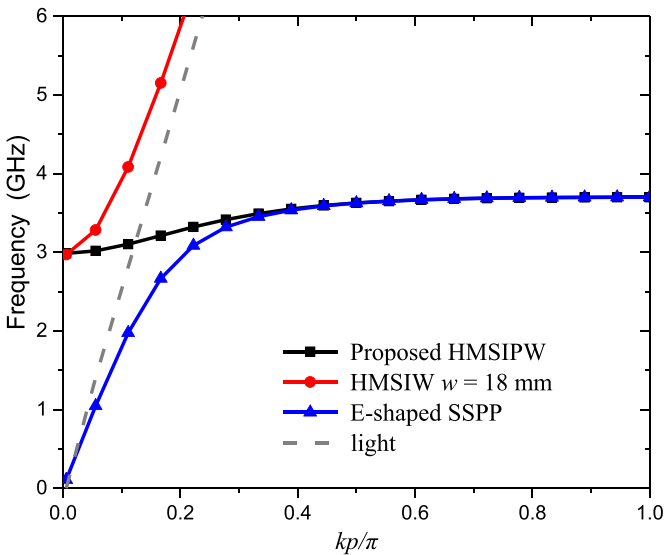


Figure 3. Dispersion curves of the proposed HMSIPW, the conventional HMSIW and the E-shaped SSPP.

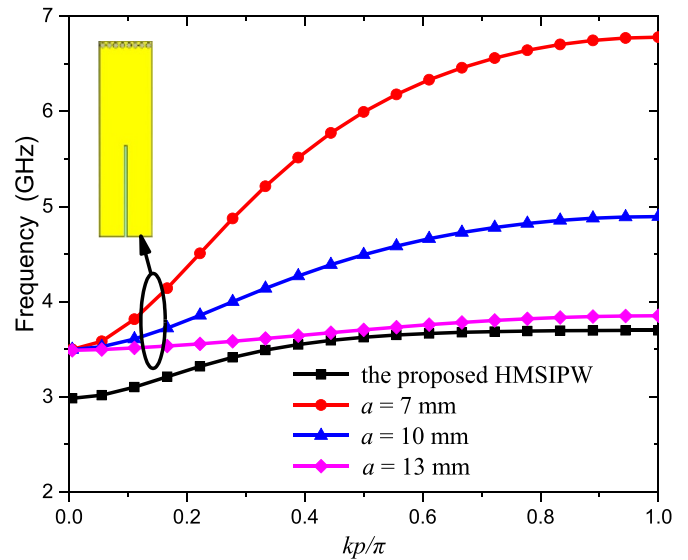


Figure 4. Dispersion curves of the conventional HMSIPW with different depths of slot and the proposed HMSIPW.

a specific passband. This method allows the lower cutoff frequency to be adjusted without changing the transversal dimension of the HMSIW, thus achieving the transversal reduction of the HMSIPW.

2.3. Simulated and measured results of the HMSIPW BPF

The manufactured prototype of the proposed HMSIPW BPF is shown in figure 5(a). Figure 5(b) illustrates the simulated and measured S-parameters of the proposed HMSIPW BPF, with

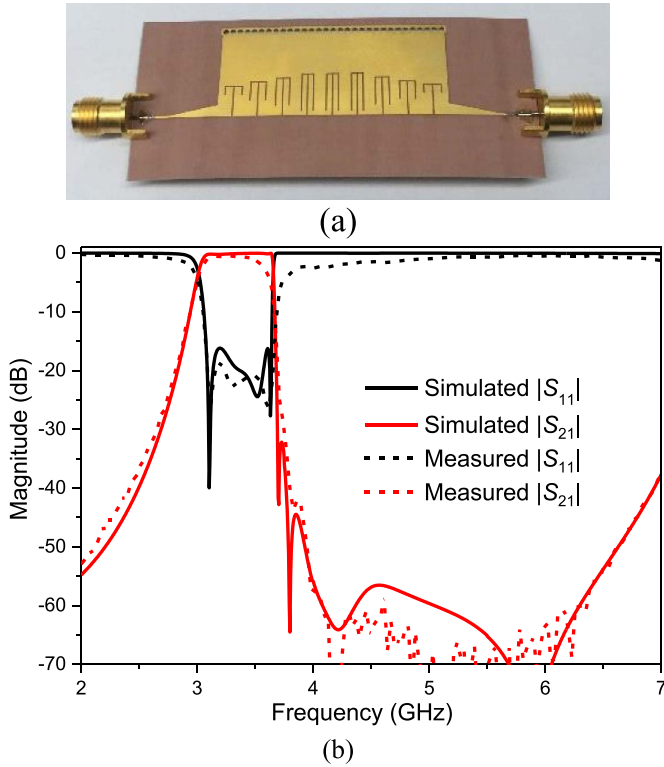


Figure 5. (a) Prototype and (b) simulated and measured S-parameters of the proposed HMSIPW BPF.

good bandpass and out-of-band rejection characteristics. The -3 dB lower and upper cutoff frequencies are 3.01 GHz and 3.66 GHz, respectively, which are almost consistent with the cutoff frequencies (2.98 GHz and 3.69 GHz) in the dispersion curve. In the passband, the reflection coefficient is lower than -16.2 dB and transmission coefficient is better than -1 dB, indicating a stable, low-loss transition. Meanwhile, in the stop-band, the transmission coefficient is lower than -40 dB from 3.93 GHz to 6.64 GHz, demonstrating a good, broadband out-of-band rejection. The measured results generally agree well with the simulated results, proving that the proposed HMSIPW has good bandpass filtering characteristics. Slight mismatching exists between the measurement and simulation results at high frequencies, which is mainly due to the fabricated tolerance and external noise.

To demonstrate the SW characteristics of the proposed HMSIPW structure, the slow-wave factor (SWF) of HMSIPW and HMSIW with the same lower cutoff frequency are compared in figure 6, where SWF is the ratio of phase velocity (v_p) to the light velocity (c) in air. In the passband of the HMSIPW BPF (3.01 GHz–3.66 GHz), the phase velocity of the HMSIPW is less than 40% of the phase velocity of the HMSIW. This indicates that the proposed HMSIPW structure reduces not only the transverse dimensions but also the longitudinal dimensions by at least 60%.

Moreover, to illustrate the propagation mechanism of the proposed HMSIPW BPF, the electric field distributions of the BPF at 3.3 GHz (in band) and 4 GHz (out of band) are shown in figures 7(a) and (b), respectively. From the comparison of the electric field distributions at two frequencies, it can be seen

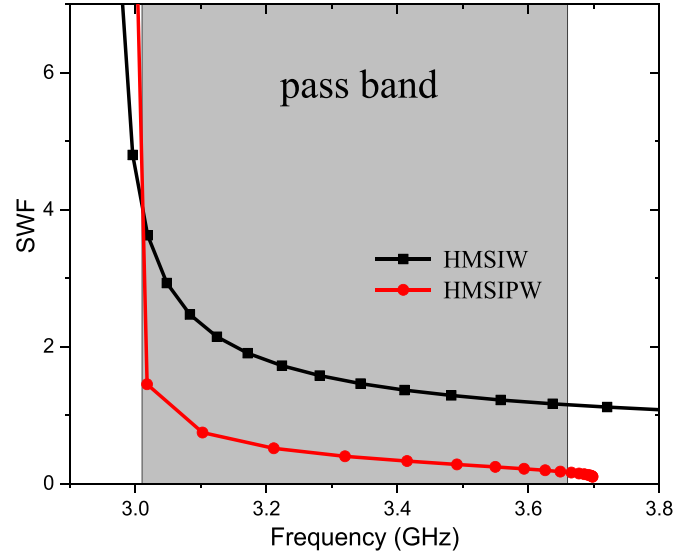


Figure 6. SWF curves of the HMSIW and the proposed HMSIPW.

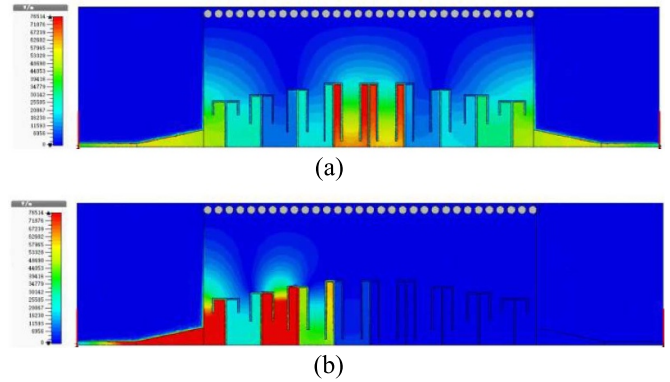


Figure 7. Top view of E-field of the proposed HMSIPW BPF at (a) 3.3 GHz and (b) 4 GHz, respectively.

that signals are successfully propagated from the input to the output at 3.3 GHz, while at 4 GHz they are blocked due to over the upper cutoff frequency of the proposed HMSIPW.

2.4. Equivalent circuit model (ECM) of the proposed HMSIPW

Based on the analysis of the dispersion curves, it can be seen that the proposed HMSIPW has features of both HMSIW and SSPP. Therefore, the principles of HMSIW [31] and SSPP [17] can be applied to guide and optimize the design of HMSIPW.

The lower cutoff frequency of the HMSIPW can be approximated by the cutoff frequency of HMSIW [31]

$$f_{c,TE_{0,5,0}} = \frac{c}{4\sqrt{\epsilon_r} \left(w - 0.54 \frac{d^2}{p} + 0.05 \frac{d^2}{2w} + \Delta w \right)} \quad (1)$$

where c is the velocity of light, ϵ_r is the relative dielectric constant of the substrate and Δw is the extra width due to edge field effect. The other parameters are consistent with the geometrical parameters of the proposed HMSIPW. However, the

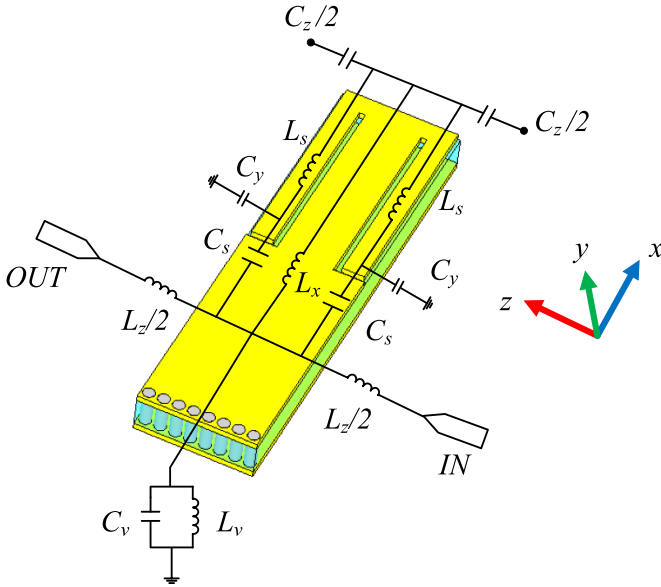


Figure 8. Equivalent circuit model of the proposed HMSIPW.

introduction of the SSPP structure changes the electromagnetic field distribution in the HMSIW [28], so that the proposed HMSIPW structure can be viewed as an HMSIW with anisotropic dielectric. Therefore, the inherent cutoff frequency of HMSIW can be modified by appropriately changing the shape and size of the SSPP structure.

To analyze the cutoff frequency of the proposed HMSIPW BPF, an equivalent circuit is developed as shown in figure 8, where the losses are not considered in order to simplify the analysis process. In figure 8, each current path on the top metallic layer of the HMSIPW (i.e. the metallic layer etched with SSPP slot lines) can be equalized as an inductor, which contains inductors L_x and L_s along the x -axis and L_z along the z -axis. The values of these inductors can be approximated by static electromagnetics [32]

$$L_x = \frac{\mu_0 b}{2\pi} \left(\ln \frac{2b}{p-c+t} + \frac{1}{2} \right) \quad (2)$$

$$L_s = \frac{\mu_0 a}{2\pi} \left(\ln \frac{2a}{\frac{c}{2} - w_s + t} + \frac{1}{2} \right) \quad (3)$$

$$L_z = \frac{\mu_0 w_s}{2\pi} \left(\ln \frac{2w_s}{w-a+t} + \frac{1}{2} \right) \quad (4)$$

where a, b, c, p, w_s are consistent with the parameters of the proposed HMSIPW, and t is the thickness of the metal layer. Since t is much smaller than the other parameters, the effect of the change in t on the equivalent inductance can be ignored. It is seen that the equivalent inductors L_x, L_s, L_z can be adjusted by changing the parameters of the SSPP slot lines in the HMSIPW structure.

On the other hand, the equivalent capacitance of the proposed structure mainly consists of two parts. One part of the capacitance is generated by the SSPP slot lines etched on the

top metallic layer (i.e. C_s and C_z in figure 8), which are positively correlated with the length of the slot lines. The other part is the capacitance generated between the top and the bottom metallic layers (i.e. C_y in figure 8), which is related to the material of the dielectric substrate, the height of the dielectric substrate and the area of the metal. Also, these equivalent capacitances can be adjusted by changing the parameters of the SSPP slotted lines.

In addition, the row of metallized via holes of the proposed HMSIPW can be seen as the capacitor and inductor connected in parallel (i.e. C_v and L_v in figure 8), and they can be defined as [33]

$$C_v = 1.41 \varepsilon_r h \quad (5)$$

$$L_v = 5.08h \left(\ln \frac{4h}{d} + 1 \right) \quad (6)$$

where ε_r is the relative dielectric constant of the substrate, h is the height of the substrate and d is the diameter of metallized via hole.

In order to analyze the characteristics of the proposed HMSIPW straightforwardly by means of ECM, the equivalent circuit is simulated and optimized with the help of the commercial software Advanced Design System. In order to verify the change effect of the SSPP structure on the cutoff frequencies by the ECM, the simulated S-parameters with different values of parameters a, b and c are shown in figure 9. The variations in the parameters a, b and c can be regarded as changes in the values of the equivalent capacitors and inductors of the ECM. When the E-shaped transversal center slot (a) increases, the L_s, L_z and C_z in the corresponding equivalent circuit increase, and the effect on the S-parameters is shown in figure 9(a). It can be seen that as L_s, L_z and C_z increase, the frequency point of the upper cutoff frequency decreases, while the lower cutoff frequency remains fixed, which coincides with the dispersion curve in figure 2(b). When the E-shaped transversal side slot (b) increases, the L_x and C_s will increase accordingly, and the effect on the S-parameters is shown in figure 9(b). Consistent with the trend of the dispersion curve in figure 2(c), as b increases (i.e. L_x and C_s increase), both of the lower and upper cutoff frequencies decrease. When the longitudinal length of the E-shaped slot (c) increases, the L_s will decrease while the L_x and C_s will increase, and the corresponding S-parameters are shown in figure 9(c). Similar to the variation effect of b , the lower and upper cutoff frequencies both decrease when c increases. Therefore, the change of S-parameters in figures 9(a)–(c) is consistent with the change of dispersion curves in figure 2, which means that the parameter changes of the SSPP structure can affect the cutoff frequencies of SSPP mode and waveguide mode. Moreover, comparison of simulated S-parameters by CST and ECM is shown in figure 9(d). It can be seen that the cutoff frequencies of the two simulation methods are in good agreement, which demonstrates the accuracy of the ECM in simulating the cutoff frequencies of the proposed HMSIPW. By adjusting the parameters of the SSPP structure (i.e. the values of a, b , and c), we can change the lower and upper cutoff frequencies of the

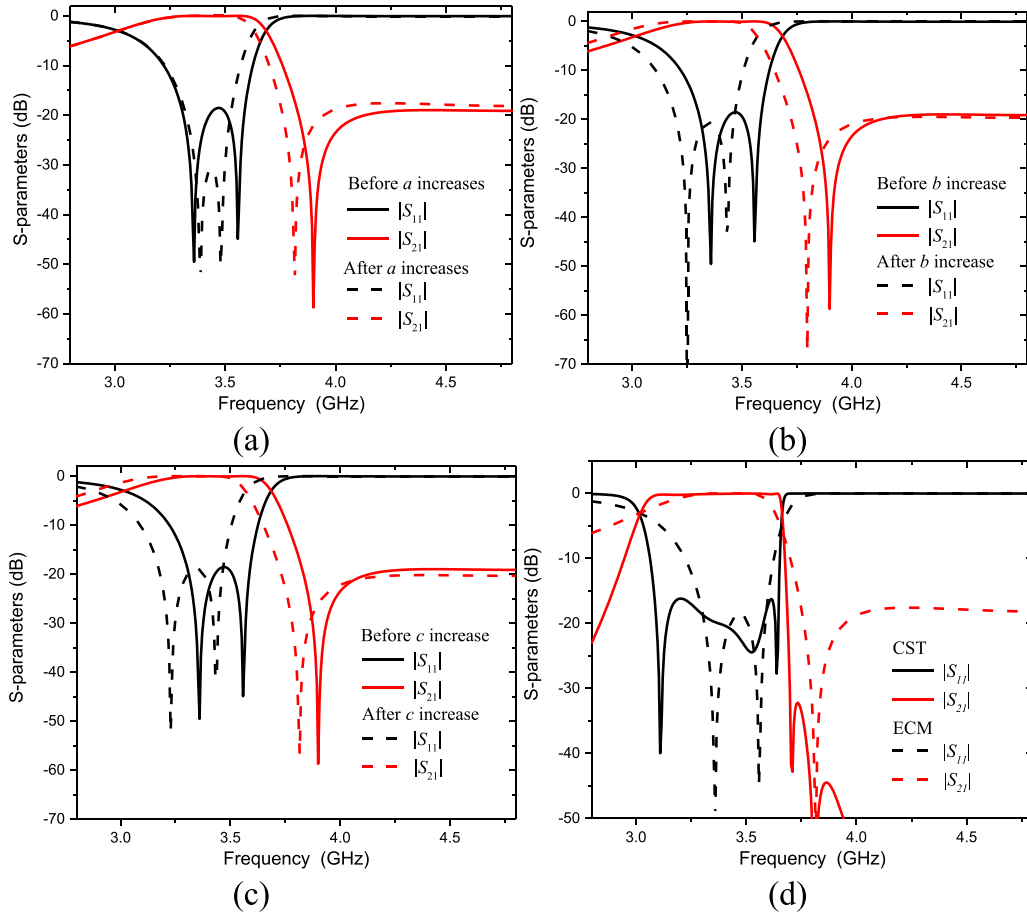


Figure 9. Simulated S-parameters of the equivalent circuit model with different (a) a , (b) b , (c) c and (d) comparison with CST.

proposed HMSIPW, thus achieving frequency and bandwidth (BW) control of passband as well as miniaturization.

3. HMSIPW diplexer

3.1. Configuration and analysis

Based on the proposed HMSIPW BPF, a diplexer is designed as shown in figure 10, which contains two bandpass filtering channels. Each channel consists of a 50 Ohm MSL, an impedance matching section and the proposed HMSIPW BPF. The two channels are combined together using a 50 Ohm T-junction to the third port. The HMSIPW BPF of Channel 1 in figure 10 with lower operating frequency is the same as described in the above section, while the BPF of Channel 2 with higher operating frequency is also based on the proposed HMSIPW. Additionally, these two BPFs are placed back to back so that the two HMSIPWs can co-share only one row of metallized via holes, further reducing the transversal dimensions of the diplexer. The prototype of the HMSIPW BPF in the Channel 2 is shown in figure 11(a), the simulated and measured S-parameters of the HMSIPW BPF in the Channel 2 are shown in figure 11(b) and the geometrical parameters of the HMSIPW BPF are given in table 2. As shown in figure 11(b),

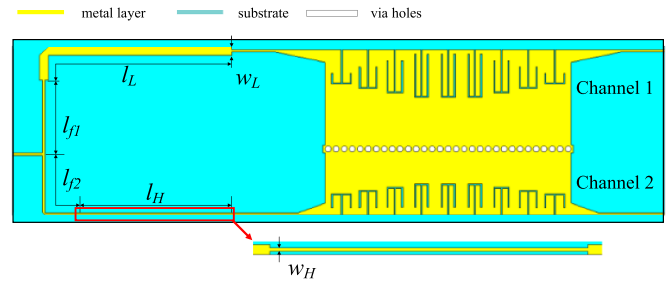


Figure 10. Configuration of the proposed diplexer. The parameters of microstrip lines are $l_{J1} = 10.93$ mm, $l_{J2} = 11.78$ mm, $l_L = 32.69$ mm, $w_L = 1.32$ mm, $l_H = 25.23$ mm, $w_H = 0.27$ mm.

the 3 dB passband of the HMSIPW BPF in the Channel 2 is 4.65 GHz–5.66 GHz, where the transmission coefficient of the HMSIPW BPF in the Channel 1 is less than -50 dB, and in contrast, the transmission coefficient of HMSIPW BPF in the Channel 2 is also less than -50 dB at the passband of the HMSIPW BPF in the Channel 1. Besides, in order to guarantee the performance of the diplexer passband, the S11 of the HMSIPW BPF in the Channel 2 passband is lower than -16 dB. The measured results are in agreement with the simulated results.

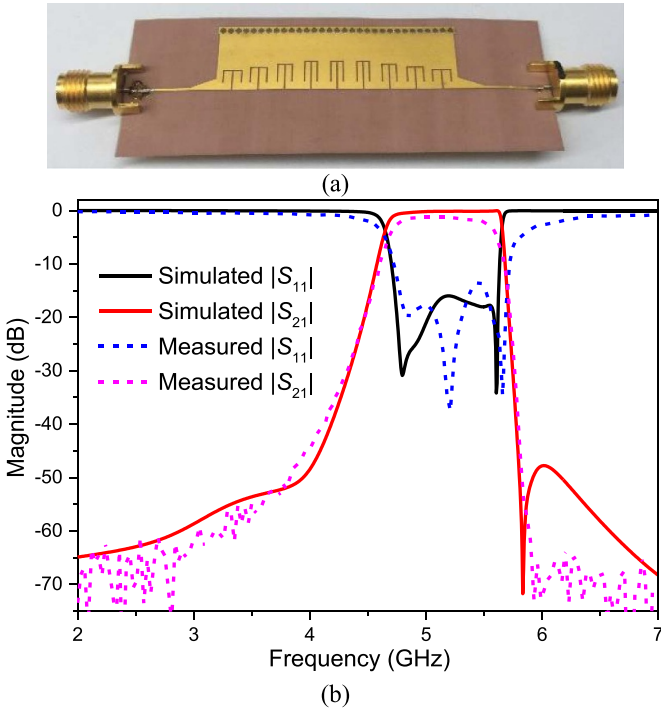


Figure 11. (a) Prototype and (b) simulated and measured S-parameters of the proposed HMSIPW BPF at higher frequency.

Table 2. Dimensions of The HMSIPW BPF Used in Channel 2.

Para.	Dim. (mm)	Para.	Dim. (mm)	Para.	Dim. (mm)
w	9.5	w_1	0.37	l_1	10
p	4	w_2	1.8	l_2	4
w_s	0.2	a_1	3	l_3	13
d	0.9	a_2	3.5	c_1	2.6
g	0.3	a_3	4	c_2	2.3
a	4.5	b_1	2.1	c_3	2
b	3.5	b_2	2.57	H	0.127
c	1.7	b_3	3.03		

The Para. in the table is the parameter and the Dim. is the dimension.

To achieve a good impedance matching, the T-junction illustrated in figure 10 needs to meet the following conditions:

$$\begin{aligned}
 Z_L &= \begin{cases} 50 \Omega & \text{at } 3.3\text{GHz} \\ \infty & \text{at } 5 \text{ GHz} \end{cases} \\
 Z_H &= \begin{cases} \infty & \text{at } 3.3\text{GHz} \\ 50 \Omega & \text{at } 5 \text{ GHz} \end{cases}
 \end{aligned} \quad (7)$$

where Z_L and Z_H are the input impedances in the direction of Channels 1 and 2 viewed from the T-junction, respectively. 3.33 GHz and 5 GHz are the center frequencies of the Channels 1 and 2, respectively. These conditions mean that the one channel of the diplexer is in the open circuited state while the other channel is in the passband, and they can be easily achieved by adjusting the length and width of the MSL between the T-junction and the BPF.

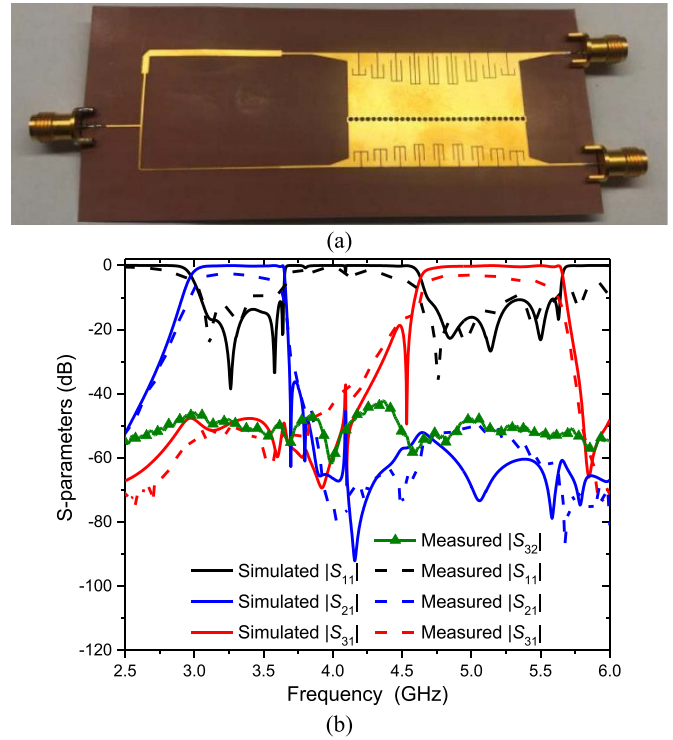


Figure 12. (a) The prototype of the proposed diplexer and (b) comparison of simulation and measurement results of S-parameters.

3.2. Simulation and measurement results

To further verify the performance of the proposed diplexer, a prototype is manufactured on the above-mentioned FSD220G substrate as shown in figure 12(a). The geometric parameters of the two HMSIPWs included in the proposed diplexer are the same as those in tables 1 and 2.

The simulated and measured S-parameters of the proposed diplexer are given in figure 12(b), where Port 2 is the output port of the Channel 1 and Port 3 is the output port of the Channel 2. As can be seen, the 3 dB passband BWs of the two channels of the diplexer are 3.02 GHz–3.66 GHz and 4.66 GHz–5.65 GHz, which are almost identical to the passbands of the two individual BPFs themselves. Good out-of-band rejection of the diplexer is achieved with below -20 dB in 3.7 GHz–4.6 GHz. Besides, a transmission zero at 4.51 GHz appears along the left edge of the passband of Channel 2, making the passband edge steeper. This is because the electromagnetic waves reflected by the BPFs of Channels 1 and 2 at this frequency have a phase difference of nearly 180 degrees, which cancel each other out, resulting in generation of the transmission zero. Moreover, the reflection coefficients S_{11} of below -10 dB at both passbands are achieved with good impedance matching. The measurement results are basically in agreement with the simulation results. The measured isolation between the two output ports (S_{32}) is below -42 dB in the whole frequency band from 2.5 to 6 GHz, indicating that the interference between the two channels of the proposed diplexer is very small and can be negligible.

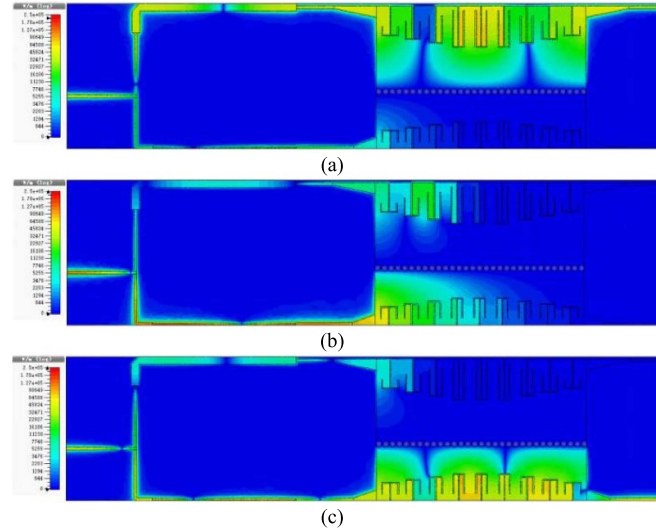


Figure 13. Top view of E-field distributions of the proposed HMSIPW diplexer at (a) 3.3 GHz, (b) 4 GHz, and (c) 5.1 GHz.

Table 3. Comparisons with previous diplexers.

Ref.	f_1/f_2 (GHz)	Type	3 dB FBW (%)	Insertion loss (dB)	Isolation (dB)	Size
[34]	26.7/28.39	SIW	4.3/1.7	3.5/4.4	34.7	$5.12 \times 3.56 (\lambda_0^2)$
[35]	1.52/1.64	Dielectric resonator	0.85/1.1	0.8/0.5	33	$0.42 \times 0.2 \times 0.16 (\lambda_0^3)$
[36]	36.15/36.65	Waveguide	1.1/1.1	2.3/2.3	30	$10.85 \times 3.62 \times 0.72 (\lambda_0^3)$
[37]	1.415/2.02	Microstrip	6.4/5	4.4/4.6	29	$0.42 \times 0.25 (\lambda_0^2)$
[38]	1/1.8	Coaxial	16/6	0.75/0.55	50	$0.873 \times 0.263 \times 0.167 (\lambda_0^3)$
This work	3.34/5.16	HMSIPW	19.16/19.2	3.6/4.2	42	$1.1 \times 0.26 (\lambda_0^2)$

The Ref. in the table is the references, FBW is the fractional bandwidth, f_1/f_2 is the center frequencies of two channels and λ_0 is the wavelength at f_1 in free space.

The electric field distributions of the diplexer at 3.3 GHz, 4 GHz and 5 GHz are shown in figure 13. At 3.3 GHz, most of the energy reaches Port 2 via the Channel 1, and barely reaches Port 3 due to the lower cutoff frequency of Channel 2 is higher than 3.3 GHz. Similarly, at 5 GHz, most of the energy reaches Port 3 via the Channel 2, but hardly ever reaches Port 2 due to 5 GHz is higher than the upper cutoff frequency of Channel 1. For the frequency at 4 GHz, the energy is reflected directly back to Port 1 and barely reaches Ports 2 and 3 due to the fact that it is located between the upper cutoff frequency of Channel 1 and the lower cutoff frequency of Channel 2. It can be seen that when one channel of the proposed diplexer is in a transmitted state, the other channel will be in a good reflective state, while both channels are in reflective states when the operating frequency is located at the out of these passbands.

Table 3 illustrates the comparisons with other types of diplexers. As can be seen, there are many advantages of the HMSIPW BPF-based diplexer, such as broad 3 dB BW, high isolation and small size. Compared with the SIW-based diplexer [34], the HMSIPW has a smaller size due to its longitudinal and transversal miniaturization features. Since the cutoff frequencies and the passband BW can be tuned by changing the size of the E-slot (a , b and c) and the width of

the HMSIPW (w), the proposed diplexer can be applied to an arbitrary frequency band and BW.

Due to the diplexer designed by the proposed HMSIPW, it also has a size reduction of more than 60% in the longitudinal direction excluding the MSL parts. Since both HMSIPWs of the diplexer co-share a row of metallized via holes, the size in the transversal direction is further reduced by 22.8%.

4. Conclusion

In this article, an HMSIPW has been proposed with low insertion loss, high out-of-band rejection, and both longitudinal and transversal miniaturization. The dispersion curve and cut-off frequency of HMSIPW can be controlled by the E-shaped SSPP structure. Simulated and measured results show that, compared with the traditional HMSIW, the size of the proposed HMSIPW is decreased by over 60% in the longitudinal dimension and 19.4% in the transversal dimension. In addition, a diplexer is designed and measured to demonstrate the application potential of the proposed HMSIPW. It has good in-band transmission and out-of-band rejection characteristics without sacrificing the performance of the proposed HMSIPW.

Data availability statement

The data that support the findings of this study are available upon reasonable request from the authors.

Acknowledgments

This work was supported in part by the FY2019 JSPS Postdoctoral Fellowship for Research in Japan under Grant P19350, in part by JST SPRING under Grant JPMJSP2114, in part by the NSAF Joint Fund under Grant U2130102, in part by the Natural Science Foundation of Shaanxi Province under Grant 2021JQ-060, and in part by the ‘Siyuan Scholar’ Fellowship of XJTU.

ORCID iD

Kai-Da Xu  <https://orcid.org/0000-0001-9408-1347>

References

- [1] Deslandes D and Wu K E 2006 *IEEE Trans. Microw. Theory Technol.* **54** 2516–26
- [2] Tan L, Xu K, Liu Y, Guo Y and Cui J 2021 *Electronics* **10** 1978
- [3] Bozzi M, Winkler S A and Wu K 2010 *IET Microw. Antennas Propag.* **4** 1965–73
- [4] Grigoropoulos N, Sanz-Izquierdo B and Young P R 2005 *IEEE Microw. Wirel. Compon. Lett.* **15** 829–31
- [5] Liu X, Wu W, Xu K, Guo Y and Chen Q 2021 *Front. Phys.* **9** 774338
- [6] Huang L and Cha H 2015 *IEEE Microw. Wirel. Compon. Lett.* **25** 223–5
- [7] Niembro-Martín A 2014 *IEEE Trans. Microw. Theory Technol.* **62** 1625–33
- [8] Jin H, Wang K, Guo J, Ding S and Wu K 2016 *IEEE Trans. Microw. Theory Technol.* **64** 1717–26
- [9] Harvey A F 1960 *IRE Trans. Microw. Theory Tech.* **8** 30–61
- [10] Xu K, Guo Y-J, Yang Q, Zhang Y-L, Deng X, Zhang A and Chen Q 2021 *IEEE Photonics Technol. Lett.* **33** 255–8
- [11] Wu J J et al 2015 *IEEE Photon. J.* **7** 1–8
- [12] Aghadjani M, Erementchouk M and Mazumder P 2016 *IEEE Trans. Terahertz Sci. Technol.* **6** 832–9
- [13] Han C, Wang Z, Chu Y, Zhao X and Zhang X 2018 *Opt. Lett.* **43** 1898–901
- [14] Ye L, Feng H, Li W and Liu Q H 2020 *J. Phys. D: Appl. Phys.* **53** 265502
- [15] Cao D, Li Y and Wang J 2017 *IEEE Antennas Wirel. Propag. Lett.* **16** 3143–6
- [16] Liu X, Feng Y, Chen K, Zhu B, Zhao J and Jiang T 2014 *Opt. Express* **22** 20107–16
- [17] Ma H, Shen X, Cheng Q, Jiang W X and Cui T J 2014 *Laser Photon. Rev.* **8** 146–51
- [18] Zhou Y J and Yang B J 2014 *Opt. Express* **22** 21589–99
- [19] Yin J Y, Ren J, Zhang Q, Zhang H C, Liu Y Q, Li Y B, Wan X and Cui T J 2016 *IEEE Trans. Antennas Propag.* **64** 5181–9
- [20] Zhu S, Liu H and Chen Z 2021 *J. Appl. Phys.* **54** 28LT02
- [21] Zhang Q, Chen B-J, Zhu Q, Chan K F and Chan C H 2019 *IEEE Antennas Wirel. Propag. Lett.* **18** 1681–5
- [22] Han Y, Gong S, Wang J, Li Y, Fan Y, Zhang J and Qu S 2020 *IEEE Trans. Antennas Propag.* **68** 3254–8
- [23] Zhong T and Zhang H 2020 *Chin. Phys. B* **29** 094101
- [24] Xu K, Lu S, Guo Y-J and Chen Q 2021 *IEEE Trans. Plasma Sci.* **49** 269–75
- [25] Guo Y, Xu K-D, Deng X, Cheng X and Chen Q 2020 *IEEE Electron Device Lett.* **41** 1165–8
- [26] Liu Y et al 2021 *IEEE Photon. Technol. Lett.* **33** 362–5
- [27] Guan D, You P, Zhang Q, Yang Z-B, Liu H and Yong S-W 2018 *IEEE Trans. Microw. Theory Technol.* **66** 2946–52
- [28] Ji L, Li X-C and Mao J-F 2020 *IEEE Trans. Microw. Theory Technol.* **68** 2539–50
- [29] Ji L, Li X-C, He X and Mao J-F 2021 *IEEE Trans. Plasma Sci.* **49** 1818–25
- [30] Cui Y et al 2020 *Asia-Pacific Microwave Conf. (APMC 2020)* pp 29–30
- [31] Lai Q, Fumeaux C, Hong W and Vahldieck R 2009 *IEEE Trans. Microw. Theory Technol.* **57** 1996–2004
- [32] Piatek Z et al 2012 *Prz. Elektron. Electr. Rev.* **88** 323–6
- [33] Jiang F 2011 *Circuit Board Design Techniques for EMC Compliance* (Beijing: China Machine)
- [34] Chi P et al 2021 *IEEE Microw. Wirel. Compon. Lett.* **31** 650–3
- [35] Xu L et al 2021 *IEEE Access* **9** 53326–32
- [36] Wu Q et al 2021 *IEEE Trans. Microw. Theory Technol.* **69** 3804–10
- [37] Chen C et al 2021 *IEEE Access* **9** 53232–42
- [38] Xie Y et al 2020 *IEEE Trans. Microw. Theory Technol.* **68** 2691–700